Topology and Secondary Structure of the N-Terminal Domain of Diacylglycerol Kinase†

Kirill Oxenoid, Frank D. Sönnichsen, and Charles R. Sanders*

Department of Physiology and Biophysics, Case Western Reserve University, Cleveland, Ohio 44106-4970

Received May 3, 2002; Revised Manuscript Received July 22, 2002

ABSTRACT: Prokaryotic diacylglycerol kinase (DAGK) functions as a homotrimer of 13 kDa subunits, each of which has three transmembrane segments. This enzyme is conditionally essential to some bacteria and serves as a model system for studies of membrane protein biocatalysis, stability, folding, and misfolding. In this work, the detailed topology and secondary structure of DAGK's N-terminus up through the loop following the first transmembrane domain were probed by NMR spectroscopy. Secondary structure was mapped by measuring ^{13}C NMR chemical shifts. Residue-to-residue topology was probed by measuring ^{19}F NMR relaxation rates for site-specifically labeled samples in the presence and absence of polar and hydrophobic paramagnetic probes. Most of DAGK's N-terminal cytoplasmic and first transmembrane segments are α-helical. The first and second transmembrane helices are separated by a short loop from residues 48 to 52. The first transmembrane segment extends from residues 32 to 48. Most of the N-terminal cytoplasmic domain lies near the interface but does not extend deeply into the membrane. Finally, catalytic activities measured for the single cysteine mutants before and after chemical labeling suggest that the N-terminal cytoplasmic domain likely contains a number of critical active site residues. The results, therefore, suggest that DAGK's active site lies very near to the water/bilayer interface.

Escherichia coli diacylglycerol kinase (DAGK)[1] resides in the plasma membrane where it catalyzes the phosphorylation of diacylglycerol as part of the membrane-derived oligosaccharide cycle, a function which is conditionally essential to cellular proliferation (*1*, *2*). DAGK is also essential to at least some Gram-positive organisms (*3*) and is important as a model system for studying membrane protein biocatalysis, stability, folding, and misfolding. DAGK catalyzes the formation of phosphatidic acid at a rate which appears to match the substrate diffusion rate limit. However, DAGK is a much slower kinase than most water-soluble kinases (*4*), possibly because the evolution-limiting rate of substrate diffusion for this reaction in vivo is the rather slow transmembrane flip-flop of diacylglycerol from the outer to inner leaflet of the plasma membrane. It has also been found that DAGK is a rather stable protein and that it is possible to generate mutants of extraordinary stability (*5*−*7*). Somewhat paradoxically, wild type and numerous mutant forms of DAGK have a high propensity to misfold into kinetically trapped aberrant conformations (*8*−*10*).

Despite years of effort, DAGK has eluded high-resolution structural determination by crystallographic or NMR methods. As a result, less direct routes to the structure are being pursued. The enzyme functions as a homotrimeric protein with three active sites per trimer (*11*, *12*). Each subunit contains 121 residues and three transmembrane segments (*13*), as summarized in Figure 1. A library of about 110 single cysteine mutant forms of DAGK is available (*5*; J. Bowie, unpublished). On the basis of the use of these mutants in conjunction with analysis of intersubunit disulfide bond formation patterns, it is believed that the second transmembrane segments from each subunit form a bundle which serves as the central 3-fold axis of symmetry in the DAGK homotrimer (*14*).

In this work, we seek to extend the existing structural model for DAGK by examining the residue-by-residue secondary structure and side chain dispositions of the 54 N-terminal residues of the protein with respect to the membrane/water interface (see Figure 1). Central to these studies is the employment of single cysteine mutants as a route to site-directed fluorine labeling, followed by ^{19}F NMR measurements in the presence and absence of topology-sensitive paramagnetic relaxation agents.

MATERIALS AND METHODS

NMR Spectral Assignment and Chemical Shift Measurements for DAGK. A stability-enhanced mutant of diacylglycerol kinase (*7*) was uniformly triply labeled with ^{2}H,

† This work was supported by the NIH (Grant RO1 GM47485) and through grants of high-field NMR spectrometer time at the Environmental Molecular Sciences Laboratory (sponsored by the U.S. DOE Office of Biological and Environmental Research) located at the Pacific Northwest National Laboratory, operated by Battelle for the DOE.

* Corresponding author. E-mail: crs4@po.cwru.edu. Phone: 615-833-3756. Fax: 615-936-2211.

[1] Abbreviations: BTFP, bromotrifluoropropanone; DAGK, diacylglycerol kinase; DM, *n*-decyl β-D-maltoside; DPC, dodecylphosphocholine; 16-DSA, 16-doxylstearate; DTNB, 5,5′-dithiobis(2-nitrobenzoic acid); DTT, dithiothreitol; EPR, electron paramagnetic resonance; Gd-DTPA, gadolinium(III) diethylenetriaminepentaacetate; POPC, 1-palmitoyl-2-oleyl-*sn*-glycero-3-phosphocholine; NMR, nuclear magnetic resonance; R_1, longitudinal relaxation rate; NOE, nuclear Overhauser effect; R_2, transverse NMR relaxation rate; SDS−PAGE, sodium dodecyl sulfate−polyacrylamide gel electrophoresis; T_1, longitudinal NMR relaxation time; T_2, transverse NMR relaxation time; TM no., transmembrane segment number; TROSY, transverse relaxation-optimized NMR spectroscopy.

10.1021/bi020335o CCC: $22.00
Published on Web 09/28/2002

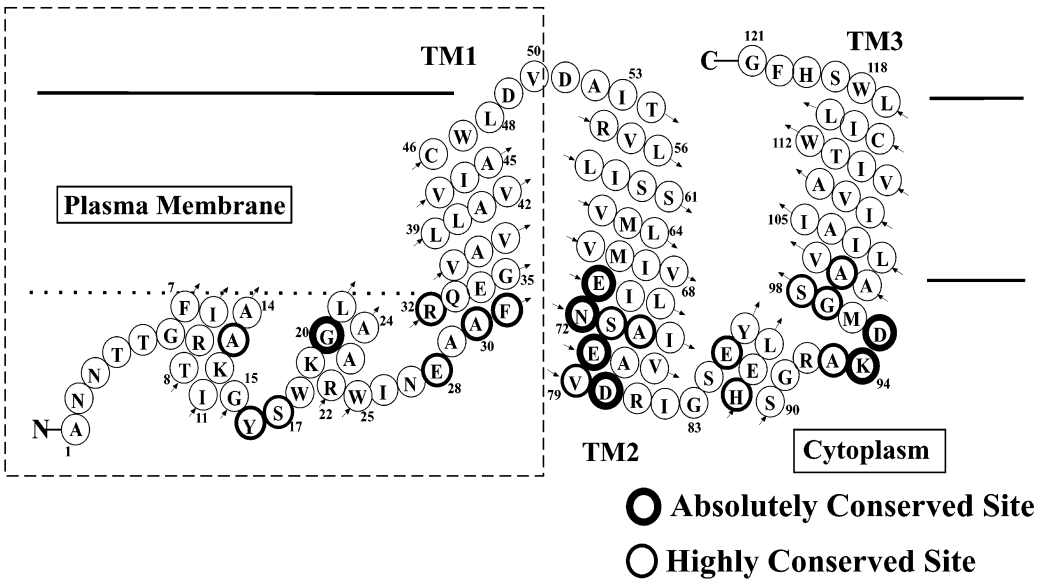

FIGURE 1: Model illustrating DAGK's sequence and membrane topology. Secondary structure and membrane topology shown for the residues within the dashed box reflect the conclusions of this study. For the C-terminal region of the protein beyond residue 54, the exact locations of helices and the beginnings and ends of transmembrane segments are not certain (see ref *13*). It is known that TM2 forms the central 3-fold axis of the native homotrimer (*14*). The bold-circled residues are observed to be highly conserved among the ca. 35 available sequences of prokaryotic DAGK (Sanders, unpublished). The residues in extra-bold circles are those which are absolutely conserved or very nearly so.

^{13}C, and ^{15}N, followed by purification in DPC micelles and sample concentration as described in ref *9*. As will be described in a separate communication, a majority of $^{13}C_\alpha$, $^{13}C_\beta$, $^{13}C'$, ^{15}N, and amide proton resonances were assigned on the basis of data from standard TROSY-based triple resonance NMR experiments conducted using a Varian (Palo Alto, CA) INOVA 800 MHz spectrometer at 45 °C (cf. refs *15*−*17*). From the same spectra used in making spectral assignments $^{13}C_\alpha$, $^{13}C_\beta$, and $^{13}C'$ chemical shifts were measured using NMRVIEW software (*18*; courtesy of Bruce A. Johnson, Merck Co., Whitehouse Station, NJ). Nuclear Overhauser effects (NOEs) between adjacent amide protons were measured as cross-peak intensities in a NOESY−TROSY experiment (*19*, *20*).

Purification of Single Cysteine DAGK Mutants. E. coli WH1061 cells overexpressing single cysteine DAGK mutants were provided by J. Bowie of UCLA (*5*). A polyhistidine purification tag was attached to the N-terminus. Thirty-five mutants were examined, each having a single Cys residue located between positions 9 and 54. Cysteine mutants for a few N-terminal sites were not probed in this work because they either expressed poorly or were unavailable. Procedures for mutant expression, purification, quantitation, and activity assay have been described elsewhere (*10*, *11*, *14*). Purified DAGK solutions contained 0.5% free dodecylphosphocholine (DPC, Anatrace, Maumee, OH), 250 mM imidazole, and 0.2 mM dithiothreitol, pH 7.8.

^{19}F Labeling and Reconstitutive Refolding. DAGK was labeled at Cys residues by thioalkylation with bromotrifluoropropanone (Indofine Chemicals, Somerville, NJ): $CF_3-CO-CH_2-Br + HS-Cys \rightarrow CF_3-CO-CH_2-S-Cys + HBr$. This reaction has previously been employed for ^{19}F labeling of proteins (*21*, *22*). BTFP was diluted 100-fold into purified DAGK samples from freshly prepared 2 M aqueous solutions. Mixtures were vigorously agitated for 1 h at room temperature, followed by reconstitutive refolding (below), during which excess reagent and small molecule side products were removed by dialysis.

Many single cysteine DAGK mutants exhibit a high propensity to misfold under standard purification procedures, such that it is necessary to apply a procedure known as "reconstitutive refolding" to generate correctly folded protein (*8*). This procedure was applied to all DAGK samples employed in this work. Briefly, it involves the addition of the phospholipid POPC (Avanti Polar Lipids, Alabaster, AL) to purified DAGK to generate DPC/POPC mixed micelles, followed by extensive dialysis to remove DPC, ultimately leading to POPC lipid vesicles containing DAGK at a 1:100 DAGK:POPC mol:mol ratio and bathed in a pH 7.8 buffer containing 10 mM imidazole and 0.05 mM EDTA. DAGK prepared using this procedure remains correctly folded even when the vesicles are redissolved by detergent to form mixed micelles (*8*).

^{19}F NMR Sample Preparation and Spectroscopy. POPC vesicles containing labeled DAGK were redissolved by adding DM from a 30% stock solution to bring the DM:POPC mol:mol ratio to 4:1. The pH of the resulting mixed micellar solution was then adjusted to 5.0 using 10% acetic acid, and the solution was concentrated by blowing filtered air over its surface at 40 °C. Final NMR samples prepared according this procedure contained 0.4 mM DAGK, 40 mM POPC, 160 mM DM, 30−50 mM imidazole, and 30−50 mM acetic acid, pH 5.0. D_2O was then added to a concentration of 10% for field-locking purposes, and trifluoroacetic acid (TFA) was added to 0.01 mM as an internal chemical shift reference. Experiments were carried out at pH 5.0 because of the favorable solubility of some mutants at that pH and to avoid the occasional formation of precipitates which sometimes occurred at higher pH values when 16-doxylstearate or Gd-DTPA was titrated into the samples.

NMR experiments were performed on a Varian 600 MHz spectrometer equipped with a Nalorac (Martinez, CA) ^{19}F/

^{1}H probe. All experiments were carried out at 30 °C. T_1 relaxation times were measured using the standard inversion recovery pulse sequence, $d_1-180-d_2-90$, with a d_1 delay of 1 s and d_2 arrayed from 1 to 60 ms. In all cases the time between scans was $\geq 4T_1$. The array covered only the initial part of the peak area vs d_2 recovery curve, since for longer d_2 the data could often not be fit by a single exponent. Such nonexponential behavior most likely resulted either from internuclear (^{19}F$-^1$H) cross-relaxation or from chemical exchange (*23*). Both effects build up and decay with time, such that they make little contribution to inversion recovery peak intensities in the short d_2 delay regime—hence our focus upon measurements made in that regime. T_1 were determined by fitting the initial rate data to a single exponent using the *xcrvfit* program (R. Boyko and B. Sykes, University of Alberta, Canada). For each mutant, T_1 were measured under three conditions: (1) without any paramagnetic probe, (2) in the presence of 1 mM gadolinium(III) diethylenetriaminepentaacetate (Gd-DTPA; Aldrich, Milwaukee, WI), and (3) in the presence of 0.5 mol % (relative to total moles of detergent and lipid) 16-doxylstearate (16-DSA; Sigma, St. Louis, MO). Gd-DTPA was added from a 100 mM stock solution while 16-DSA was added from 100 mM solutions which also contained 30% DM to solubilize this hydrophobic probe.

DAGK Cross-Linking and Cysteine Modification Rate Measurements. Nonspecific cross-linking of the normally homotrimeric DAGK was carried out using glutaraldehyde (GA, Sigma). One volume of vesicle-reconstituted DAGK was diluted into 9 volumes of 1% DM and 40 mM imidazole/acetic acid, pH 5.0. GA was added to 16 mM, and the mixture was vigorously agitated for 24 h, followed by SDS−PAGE using a 4−12% NuPAGE Bis-Tris gel (Invitrogen, Carlsbad, CA).

For cysteine modification rate measurements 1 mg/mL solutions of DAGK in DM/POPC mixed micelles (15 mol % POPC) were reacted with DTNB at 30 °C. The initial rates of the reactions were extracted from the time dependence of light absorbance at 405 nm resulting from the appearance of the thionitrobenzoate anion. The detailed methods are presented in ref *24*.

Theory of Paramagnet Perturbation of NMR Relaxation Rates. Unpaired electron dipole-induced nuclear relaxation rates are inversely proportional to the sixth power of the distance between the spins (*25*). In the diffusion-controlled regime, the radius of nucleus−electron interaction fluctuates between the distance of closest approach, d, and infinity and has to be averaged (*26*). The type of integration required depends on spatial distribution of the paramagnetic species around the nucleus of interest. In the simplest case of an isotropic distribution of paramagnetic molecules for which the electron spin relaxation time τ_s is much shorter than translational diffusion time constant τ_D, conventional Solomon equations for T_1 and T_2 can be used, with τ_s playing the role of correlation time and $1/r^6$ being averaged between d and infinity. On the other hand, if $\tau_D \ll \tau_s$, the formulas for T_1 and T_2 will contain spectral density functions that depend on τ_D. Under the conditions of the experiments of this work, it is quite possible that for each probe τ_D and τ_s are of comparable magnitude (roughly 10^{-8} s for the micelle-associated 16-DSA and 10^{-10} s for the soluble Gd-DTPA), so that neither limiting condition is satisfied. For this reason and also due to the variable local concentrations of the spin probes with respect to a given ^{19}F label/residue, quantitative analysis has not been undertaken. Rather, we interpret the data much more conservatively, comparing data from site to site as an indicator of the relative access of the probe to ^{19}F-labeled side chains.

RESULTS

Secondary Structure of Residues 1−54. As summarized in Materials and Methods, a majority of backbone and $^{13}C_\beta$ NMR resonances of DAGK in DPC micelles have been assigned using standard TROSY-based triple resonance NMR methods (cf. refs *15*−*17*). For the assigned $^{13}C_\alpha$ and $^{13}C'$ resonances, differences between the observed and random coil chemical shifts are reported in Figure 2. It is now well-established that such differential shifts (especially for $^{13}C_\alpha$) are reliable indicators of protein secondary structure (*27*). On the basis of the positive deviation of the $^{13}C_\alpha$ differential shift from the random coil range, it appears that residues 6−15, 18−25, and 29−47 represent helical segments. DAGK's second transmembrane segment appears to be initiated as a helix starting at residue 52. These observations are generally supported by the less conclusive $^{13}C'$ data.

NOESY experiments were also carried out to measure NOEs between amide protons. The possibility of measuring NOEs between other classes of protons was ruled out because perdeuterated protein was used in which the only protons are the back-exchanged amide protons. Observation of NH_i-NH_{i+1} NOEs between adjacent residues is consistent with, but does not prove, helical secondary structure (*20*). However, the *absence* of such NOEs can be taken as an indication of nonhelical structure. Results from the NOE experiments are shown in Figure 2 and support the interpretation of the chemical shift data that there is a break between helices located at residues 16−18 between α-helices and that the first transmembrane segment terminates at residue 48. In the case of the apparent break or turn between helices at residues 27 and 28, the NOE data neither support nor dispute the chemical shift data, although additional support for a break or kink at this position comes from the ^{19}F data (below).

^{19}F Labeling of DAGK. DAGK was initially ^{19}F-labeled using trifluoroethylthiosulfonate, which led to mixed disulfides with cysteine side chains. This method was recently employed in studies of rhodopsin by the Khorana laboratory (*29*, *30*). However, it was observed that the disulfide bonds formed by this method tended to undergo spontaneous reduction over a period of hours, even in the absence of a reducing agent. This method was therefore abandoned in favor of irreversible thioalkylation using 3-bromo-1-trifluoropropanone (*21*, *22*). By measuring the residual −SH present following reaction, the efficiency of labeling was observed to vary between 36% and 85% depending on site, with a mean of 63%.

The activity of each ^{19}F-labeled DAGK mutant was measured and compared to that of an unlabeled control (Figure 3). Labeling sometimes resulted in a considerable reduction in activity compared to that of the unmodified mutant. In general, reductions in DAGK activity due to labeling may reflect any of the following: (1) a structural perturbation leading indirectly to a loss of activity, (2) direct perturbation of the enzyme active site, or (3) perturbation of protein folding so that the labeled mutant does not fold

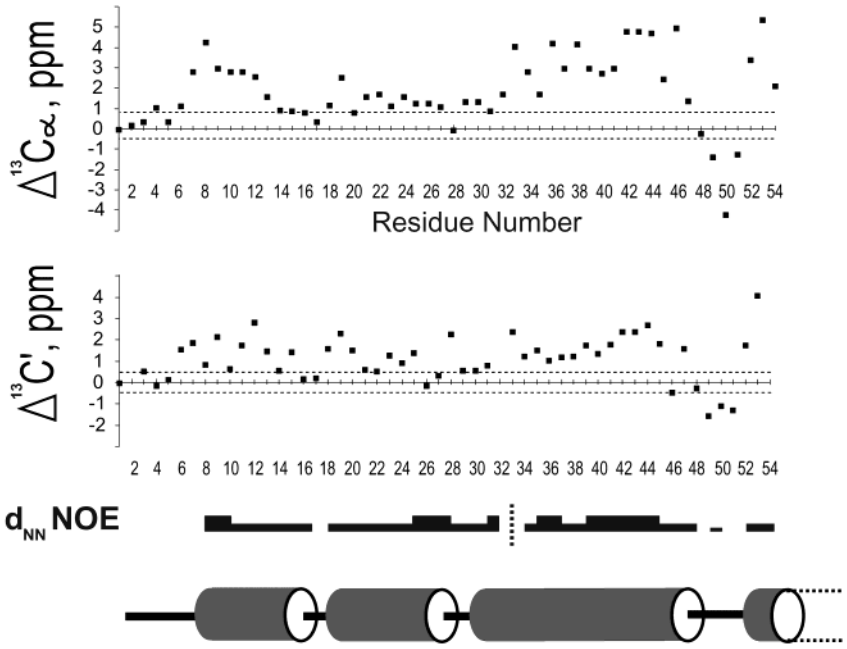

FIGURE 2: ^{13}C NMR secondary chemical shifts (observed shift minus random coil value), NH_i-NH_{i+1} NOEs, and derived secondary structure diagram for sites 1−54 of DAGK. In the chemical shift plots, the area within the dashed lines around the *X* axis defines the range of random coil shifts: −0.5 to +0.8 ppm for $^{13}C_\alpha$ and −0.5 to +0.5 ppm for $^{13}C'$ (*25*). For both $^{13}C_\alpha$ and $^{13}C'$, positive chemical shifts outside the random coil range are indicative of α-helical structure. The amide−amide proton NOEs are classified as strong, medium, and weak on the basis of the intensities of cross-peaks relative to the intensities of diagonal peaks, which is reflected in the thickness of the bar between adjacent residues. In the cases of the amide proton at site 33, it was impossible to measure NOEs because its resonance was not assigned (although the $^{13}C_\alpha$ and $^{13}C'$ resonances for that position were assigned using HNCO/HNCOCA experiments). In the secondary structure diagram, cylinders represent α-helices; the rest are loops or unstructured elements. $^{13}C'$ shifts for residues N2, R32, and R54 are not presented because their resonance assignments are ambiguous.

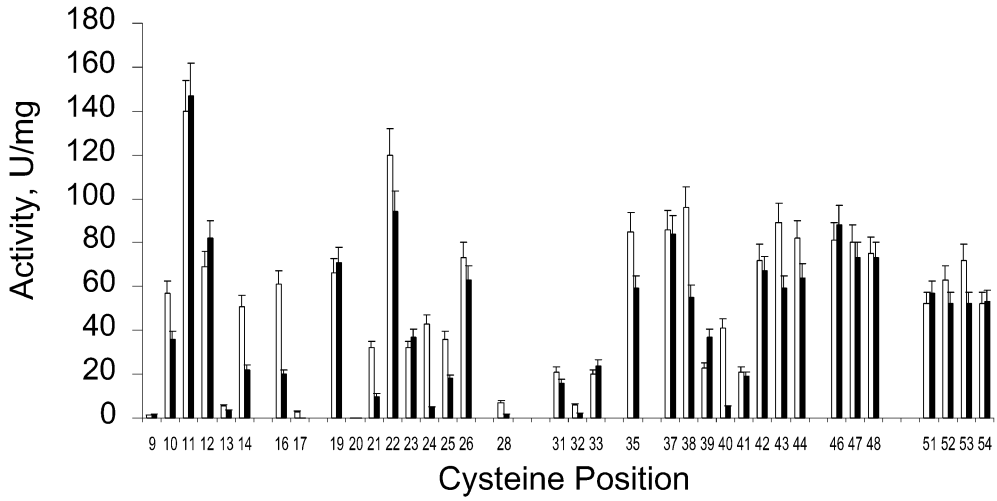

FIGURE 3: Catalytic activities for refolded DAGK single cysteine mutants measured before (open bars) and after (closed bars) thioalkylation with BTFP.

properly. To gain insight into which explanation most likely pertains, we carried out chemical cross-linking on the labeled mutants. Following cross-linking with glutaraldehyde, correctly folded DAGK exhibits a distinctive SDS−PAGE profile whereby an intense trimer band is observed along with residual monomer and dimer bands (see control lane in Figure 4). It has been shown that single cysteine DAGK mutants which are contaminated with misfolded protein usually exhibit cross-linking patterns in which the trimeric band is *not* the most intense and/or in which oligomers higher than trimer are observed (*8*). Moreover, DAGK's tertiary and quaternary structures are coupled, such that any global conformational perturbation is likely to be accompanied by a change in quaternary structure (*8*). GA cross-linking may therefore be used to identify samples which contain significant quantities of residual misfolded DAGK or in which the protein has undergone a major probe-induced structural perturbation. Representative results appear in Figure 4. Out of 32 mutants tested, only mutants 40 and 52 exhibited unusual gel patterns (with 40 giving an unusual pattern even without labeling, suggesting misfolding). Therefore, for most sites there was clearly no global perturbation of either folding efficiency or protein structure due either to mutation to Cys or to subsequent thioalkylation.

^{19}F NMR Measurements in the Presence and Absence of Paramagnetic Probes. NMR spectra of an ^{19}F-labeled DAGK

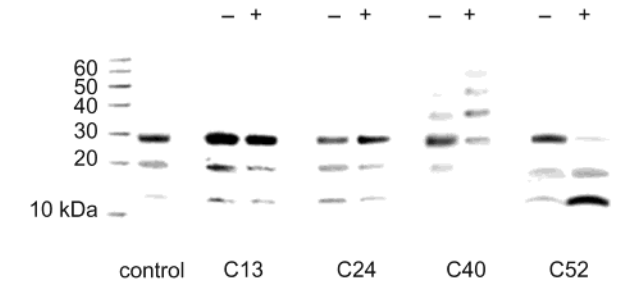

FIGURE 4: GA cross-linking results for selected single cysteine mutants before (−) and after (+) thioalkylation with BTFP. Control: cross-linked WT DAGK. The normal cross-linking patterns exemplified by mutants 13 and 24 were observed for 35 out of 37 mutants, both before and after thioalkylation. Mutants 40 and 52 are the two abnormal cases.

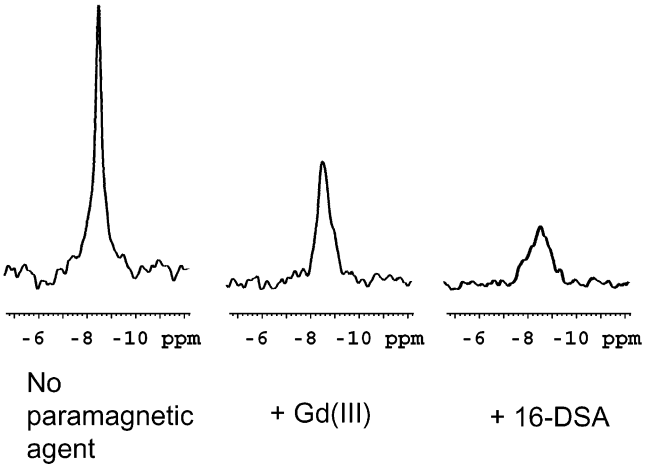

FIGURE 5: Representative ^{19}F NMR spectra of DAGK in the presence and absence of paramagnetic probes. These data are for the site 17 cysteine mutant.

single cysteine mutant in DM/POPC mixed micelles in the presence of the water-soluble paramagnetic probe Gd-DTPA or the hydrophobic 16-DSA are shown in Figure 5. Both probes have previously been used as relaxation agents in NMR studies of membrane-associated proteins (cf. refs *31* and *32*). 16-DSA was preferred to 5-doxylstearate as a lipophilic probe because the addition of the latter reagent to DAGK often resulted in the formation of a precipitate. Gd-DTPA was chosen instead of 4-amino-TEMPO as a polar probe because this latter reagent was observed to have a significant affinity for micelles, as previously observed for other TEMPO derivatives (*33*). In the case of the Gd-DTPA complex, the possibility that the single unligated coordination site on Gd(III) might preferentially bind to protein carboxyl moieties (cf. ref *34*) was reduced by maintaining a significant free acetate concentration in the samples (ca. 40 mM). Longitudinal relaxation rates (R_1) were measured in the presence and absence of these reagents.

The ΔR_1 data illustrated in Figure 6 clearly distinguish the N-terminal cytoplasmic domain (sites 9−31) from the first transmembrane domain (sites 32−48). Sites in TM1 exhibited very low exposure to Gd-DTPA, while sites in the cytoplasmic domain generally exhibited much higher degrees of exposure to Gd-DTPA and lower exposure to the hydrophobic 16-DSA. The end of TM1 near residue 48 is also obvious from these data. Within the cytoplasmic domain there was generally a strong *inverse* correlation between the magnitudes of ΔR_1 for Gd-DTPA as compared to 16-DSA for each site, suggesting that water/micelle disposition is the primary determinant of site-specific access by the two probes.

Confirmation of the Loop Connecting TM1 and TM2 by Chemical Modification Rate Measurements. The chemical shift and NOE data of Figure 2 and the ^{19}F NMR data indicate that the loop connecting the first and second transmembrane segments of DAGK is located in the 48−51 sequential region. This was verified by chemical modification rate data for the reactions of DTNB with the cysteine mutants for these sites, as illustrated in Figure 7.

DISCUSSION

Backbone NMR spectral assignments have been completed for residues located in DAGK's N-terminal domain such that it is possible to map its secondary structure on the basis of chemical shift analysis and interresidue NOEs (Figure 2). Supplementing and complementing these data are ^{19}F NMR relaxation measurements in which the access of site-directed ^{19}F labels to polar and lipophilic paramagnetic probes was examined (Figure 6). These measurements are analogous to widely employed EPR methods in which spectra of site-directed spin labels are examined in the presence and absence of paramagnetic probes (*35*−*37*). Such measurements can, ideally, illuminate side chain disposition with respect to both the water/membrane interface and the protein/medium (lipid or water) interfaces (*35*−*37*).

Secondary Structure and Topology of Transmembrane Segment 1. The chemical shift and NOE data indicate that an α-helix extends from residues 29 to 47. This helix starts outside of the membrane but comprises most of DAGK's first transmembrane segment, which appears to extend from sites 32 to 48 on the basis of the ^{19}F ΔR_1. The fact that sites 29−32 are located at or just above the water/membrane interface is significant since A30, F31, and R32 are all highly conserved residues which are most likely part of DAGK's active site (see below). This suggests that an important role for TM1 is to anchor part of DAGK's active site at a well-ordered juxtamembrane location.

The ^{13}C NMR, NOE, ^{19}F NMR, and chemical modification rate data indicate the presence of a short water-exposed loop/turn spanning residues 48 through 52, with site 51 being the most highly water-exposed site. These data also suggest that, while the helix of TM1 terminates before it reaches the aqueous phase, the helix of TM2 is initiated at site 52 in a more highly water-exposed region of the interface. Given that DAGK serves as a model system for studies of transmembrane protein insertion (*10*, *38*), identification of the exact location of the loop connecting transmembrane segments 1 and 2 may provide a rational basis for future mutagenesis studies to probe the structural features which determine DAGK's bilayer insertion rate.

Within TM1, there was considerable variation from 16-DSA-induced ΔR_1 (Figure 6). Those sites exhibiting the largest ΔR_1 (e.g., sites 35 and 37) are probably fully exposed to the hydrocarbon interior of the micelles, while other sites (e.g., sites 38 and 39) are shielded from the probe by protein−protein interactions with other transmembrane segments of the protein. However, the periodicity of the 16-DSA ΔR_1 data for TM1 helical sites was not well fit by a sinusoidal function having a periodicity of 3.6 residues (not

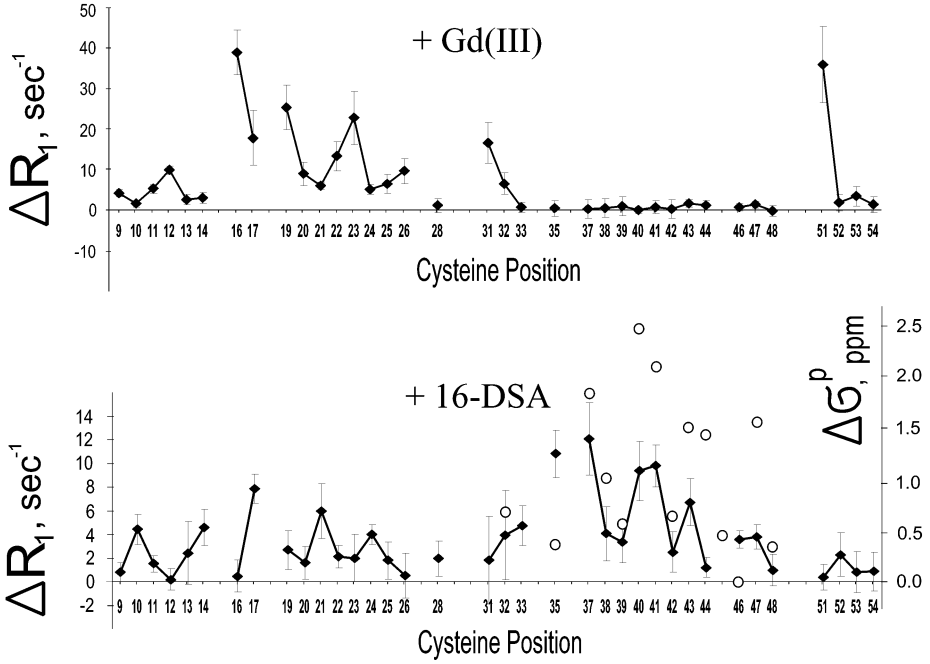

FIGURE 6: Changes in the ^{19}F longitudinal relaxation rates (ΔR_1) induced by paramagnetic probes as a function of the site of labeling (closed diamonds: top, effect of 1 mM Gd(III), bottom, effect of 1 mM 16-DSA). Cysteine mutants for sites not represented by data in this figure either expressed poorly or were not available. Included in the bottom panel for comparison is the effect of pressurized oxygen on the ^{19}F chemical shift for the transmembrane residues as originally reported in Luchette et al. (*39*; open circles). These $\Delta\sigma^p$ represent the difference between shifts measured at 100 atm of O_2 and at ambient pressure.

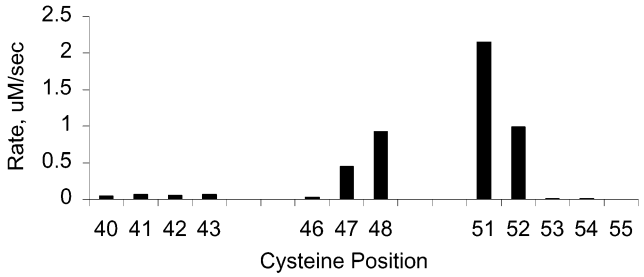

FIGURE 7: Initial rates (micromolar per second) of chemical modification by Ellman's reagent of cysteine sites in the loop connecting TM1 and TM2.

shown), as would be expected for the ideal case where there is a single lipid-exposed face along the long axis of a helix (cf. ref *39*). One possible explanation is that the lipid/protein interactions of this segment are more complicated than as described by a single face-buried model. Alternatively, 16-DSA and trifluoropropanone may not be ideal probes for mapping site dispositions within transmembrane domains. This latter interpretation is supported by results from the recent work of Luchette et al. (*37*) in which the TM1 region of DAGK was examined using the same ^{19}F labeling method but using pressurized molecular oxygen as the paramagnetic probe. In that study, the oxygen perturbation of ^{19}F chemical shifts for sites in TM1 (illustrated in Figure 6) fit reasonably well to a sinusoidal function having a periodicity of 3.6. Since both the previous study and the present work employed the same DAGK mutants and the same ^{19}F labeling method, this result suggests that TM1 may indeed have a single lipid-exposed face along its long axis but that O_2 may be a much more ideal probe for residue disposition within the membrane than 16-DSA. This would not be surprising since O_2 is a much smaller and more symmetric hydrophobic probe than 16-DSA.

Secondary Structure and Topology of the N-Terminal Cytoplasmic Domain. From the generally higher Gd-DTPA-induced ΔR_1 of residues 9−28 (Figure 6), it is clear that this segment is much more highly exposed to water than sites in TM1, indicating that this domain does not undergo interactions with the micelles which extend deeply into the hydrophobic interior. The fact that some sites (10, 14, 17, and 21) are also well exposed to the lipophilic 16-DSA argues in favor of a water/micelle interfacial location. The chemical shift and NOE data indicate that residues 8−16 and 18−25 are helical segments, separated from each other and from the first transmembrane helical segment starting at residue 29 by short loops or kinks. The ΔR_1 data patterns exhibited by the residues in these two helices are consistent with the possibility that they are surface-associated amphipathic helices. For the latter of these two helices there must be a turn or major kink connecting it to the adjacent (and roughly perpendicular) transmembrane segment, as supported by the chemical shift data.

The conclusion that the N-terminal cytoplasmic domain of DAGK is dominated by two helices which are located at or very near the water/bilayer interface is important since a number of highly conserved residues are found within this segment (Figure 1), some of which are part of DAGK's active site (*12* and see below). These results mirror conclusions regarding the interfacial location of active site residues 30−32 and strongly suggest that most or all of DAGK's active site is located near the water/bilayer interface. While this might be expected for an enzyme which catalyzes direct transfer of a phosphoryl moiety from a water-soluble donor (MgATP) to a lipid acceptor (DAG), it is interesting that this active site disposition is very different from that observed for the cyclooxygenases (*40*) and for some phospholipases (*41*). Both enzymes also execute chemical transformations of lipids but have active sites located well above the

membrane surface, to which lipid substrates must diffuse through hydrophobic protein channels.

Tentative Identification of Active Site Residues in the N-Terminal Domain. A number of unlabeled single cysteine mutants exhibited catalytic activities of <10% of wild-type activity (ca. 100 units/mg, Figure 3). These include mutants for sites 9, 12, 17, 20, 28, and 32. Most of these sites are evolutionarily highly conserved (see Figure 1). While possible roles in catalysis for these sites will require verification and elaboration, Cys replacement mutants for these sites were observed to be structurally similar to WT, consistent with primarily catalytic rather than structural roles. For most of those low activity mutants, thioalkylation resulted in additional losses of catalytic activity. For sites retaining >10% of wild-type activity following mutation to cysteine, subsequent thioalkylation resulted in >50% losses of activity in the cases of mutants 14, 16, 21, 24, and 40. Among these, a gross structural perturbation was observed only for the site 40 mutant, which exhibited a defective oligomeric state even before labeling (Figure 4). Since the other four sites are all sequentially proximal to putative active site residues, these label-induced activity losses most likely result from active site perturbations. It is perhaps not surprising that sites in TM1 are generally tolerant of mutation to cysteine and to subsequent thioalkylation since none of its sites are highly conserved (Figure 1) and since TM1 can be mutated to polyalanine with a resulting activity loss of only about 50% (*42*). The results of this work establish which sites are sensitive to mutation and/or labeling and are therefore targets for more detailed characterization in the future.

ACKNOWLEDGMENT

We thank James Bowie and laboratory group at UCLA for providing most of the mutants employed in this project, David Hoyt for assistance with the NMR experiments run at the EMSL facility, and Bonnie Gorzelle for excellent technical assistance and proofreading. We also thank Lech Czerski for carrying out the chemical modification rate measurements, Scott Prosser and David Cafiso for helpful discussion, and Lewis Kay of the University of Toronto for making available the TROSY-based NMR sequences.

REFERENCES

1. Kennedy, E. P. (1996) in *E. coli and S. typhimurium: Cellular and Molecular Biology* (Neidhardt, F. C., Ed.) 2nd ed., Vol. I, pp 1064−1071, ASM Press, Washington, DC.
2. Raetz, C. R. H., and Newman, K. F. (1978) *J. Biol. Chem. 253*, 3882−3887.
3. Yamashita, Y., Takehara, T., and Kuramitsu, H. K. (1993) *J. Bacteriol. 175*, 6220−6228.
4. Badola, P., and Sanders, C. R. (1997) *J. Biol. Chem. 272*, 24176−24182.
5. Lau, F., and Bowie, J. U. (1997) *Biochemistry 36*, 5884−5892.
6. Lau, F. W., Nauli, S., Zhou, Y., and Bowie, J. U. (1999) *J. Mol. Biol. 290*, 559−565.
7. Zhou, Y., and Bowie, J. U. (2000) *J. Biol. Chem. 275*, 6975−6979.
8. Gorzelle, B. M., Nagy, J. K., Oxenoid, K., Lonzer, W. L., Cafiso, D. S., and Sanders, C. R. (1999) *Biochemistry 38*, 16373−16382.
9. Oxenoid, K., Sonnichsen, F. D., and Sanders, C. R. (2001) *Biochemistry 40*, 5111−5118.
10. Nagy, J. K., Lonzer, W. L., and Sanders, C. R. (2001) *Biochemistry 40*, 8971−8980.
11. Vinogradova, O., Badola, P., Czerski, L., Sonnichsen F. D., and Sanders, C. R. (1997) *Biophys. J. 72*, 2688−2701.
12. Lau, F. W., Chen, X., and Bowie, J. U. (1999) *Biochemistry 38*, 5521−5527.
13. Smith, R. L., O'Toole, J. F., Maguire, M. E., and Sanders, C. R. (1994) *J. Bacteriol. 176*, 5459−5465.
14. Nagy, J. K., Lau, F., Bowie, J. U., and Sanders, C. R. (2000) *Biochemistry 39*, 4154−4164.
15. Wider, G., and Wuthrich, K. (1999) *Curr. Opin. Struct. Biol. 9*, 594−601.
16. Salzmann, M., Wider, G., Pervushin, K., Senn, H., and Wuthrich, K. (1999) *J. Am. Chem. Soc. 121*, 844−848.
17. Pervushin, K., Riek, R., Wider, G., and Wuthrich, K. (1997) *Proc. Natl. Acad. Sci. U.S.A. 94*, 12366−12371.
18. Johnson, B. A., and Blevins, J. (1994) *J. Biomol. NMR 4*, 603−614.
19. Barsukov, I. L., and Lian, L.-Y. (1993) in *NMR of Macromolecules. A Practical Approach* (Roberts, G. C. K., Ed.) pp 335−339, Oxford University Press, Oxford.
20. Wüthrich, K. (1986) in *NMR of Proteins and Nucleic Acids*, pp 162−175, Wiley, New York.
21. Huestis, W. H., and Raferty, M. A. (1972) *Biochemistry 11*, 1648−1654.
22. Brauer, M., and Sykes, B. D. (1986) *Biochemistry 25*, 2187−2191.
23. Banci, L., Bertini, I., and Luchinat, C. (1991) in *Nuclear and Electron Relaxation*, pp 48−52, VCH, New York.
24. Czerski, L., and Sanders, C. R. (2000) *FEBS Lett. 472*, 225−229.
25. Peters, J. A., Huskens, J., and Raber, D. J. (1996) *Prog. NMR Spectrosc. 28*, 283−350.
26. Abragam, A. (1994) in *Principles of Nuclear Magnetism*, pp 300−305, Oxford University Press, Oxford.
27. Wishart, D. S., and Sykes, B. D. (1994) *Methods Enzymol. 239*, 363−392.
28. Spera, S., and Bax, A. (1991) *J. Am. Chem. Soc. 113*, 5490−5492.
29. Klein-Seetharaman, J., Getmanova, E. V., Loewen, M., Reeves, P. J., and Khorana, H. G. (1999) *Proc. Natl. Acad. Sci. U.S.A. 96*, 13744−13749.
30. Loewen, M., Klein-Seetharaman, J., Getmanova, E. V., Reeves, P. J., Schwable, H., and Khorana, H. G. (2001) *Proc. Natl. Acad. Sci. U.S.A. 98*, 4888−4892.
31. Danielson, M. A., and Falke, J. J. (1996) *Annu. Rev. Biophys. Biomol. Struct. 25*, 163−195.
32. Papavoine, C. H. M., Konings, R. N. H., Hilbers, C. W., and van de Ven, F. J. M. (1994) *Biochemistry 33*, 12990−12997.
33. Almeida, L. E., Borissevitch, I. E., Yushmanov, V. E., and Tabak, M. (1998) *J. Colloid Interface Sci. 203*, 456−463.
34. Petros, A. M., Mueller, L., and Kopple, K. D. (1990) *Biochemistry 29*, 10041−10048.
35. Hubbell, W. L., Cafiso, D. S., and Altenbach, C. (2000) *Nat. Struct. Biol. 7*, 735−739.
36. Hubbell, S. L., Gross, A., Langen, R., and Lietzow, M. A. (1998) *Curr. Opin. Struct. Biol. 8*, 649−656.
37. Perozo, E., Cortes, D. M., and Cuello, L. L. (1998) *Nat. Struct. Biol. 5*, 459−469.
38. Sanders, C. R., Czerski, L., Vinogradova, O., Badola, P., Song, D., Smith, S. O. (1996) *Biochemistry 35*, 8610−8618.
39. Luchette, P. A., Prosser, R. S., and Sanders, C. R. (2002) *J. Am. Chem. Soc. 124*, 1778−1781.
40. Picot, D., Loll, P. J., and Garavito, R. M. (1994) *Nature 367*, 243−249.
41. Roberts, M. F. (1999) in *Introduction to Cellular Signal Transduction* (Sitaramayya, A., Ed.) pp 89−146, Birkhauser, Boston.
42. Zhou, Y., Wen, J., and Bowie, J. U. (1997) *Nat. Struct. Biol. 4*, 986−990.

BI020335O